Au Nanoparticle Modified WO 3 Nanorods with Their Enhanced Properties for Photocatalysis and Gas Sensing

ARTICLE *in* THE JOURNAL OF PHYSICAL CHEMISTRY C · FEBRUARY 2010

Impact Factor: 4.77 · DOI: 10.1021/jp909742d

Au Nanoparticle Modified WO_3 Nanorods with Their Enhanced Properties for Photocatalysis and Gas Sensing

Q. Xiang,[†,‡] G. F. Meng,[†] H. B. Zhao,[†] Y. Zhang,[†] H. Li,[†] W. J. Ma,[†] and J. Q. Xu*[,†,‡]

Department of Chemistry, College of Science, Shanghai University, Shanghai 200444, China, and State Key Laboratory of Transducer Technology, Shanghai Institute of Microsystem and Information Technology, Chinese Academy of Sciences, Shanghai 200050, China

Received: October 11, 2009; Revised Manuscript Received: December 17, 2009

A novel photocatalysis and gas sensing material was synthesized by decorating Au nanoparticles on tungsten trioxide nanorods. Tungsten trioxide nanorods were prepared through the ion-exchange method combined with hydrothermal treatment and further modified with Au nanoparticles (Au NPs). After Au NPs decorated on the surface of WO_3 nanorods (WO_3 NRs), the reducing gas (hydrogen, methanol, ethanol, etc.) sensing properties and the photocatalytic performance of rhodamine B (RhB) were all greatly improved. Au NP modified WO_3 nanorods (Au NP@WO_3 NRs) exhibit not only larger response (H_2 50 ppm, recovery time lower than 10 s) and better selectivity (Ra/Rg = 6.6) for H_2 gas detection than pure WO_3 NRs but also high photocatalytic properties for the absolute degradation of RhB under simulated sunlight irradiation for 120 min.

1. Introduction

With the improvement of living standards, the need for good environment quality has been inadvertently heightened. The effective detection of toxic and hazardous gases, as well as the degradation of organic pollutants has become imperative. In recent years, tungsten oxide has attracted great attentions for its distinctive photocatalytic and electrochromic properties.[1−4] It is regarded as a promising material for a multitude of potential applications including semiconductor gas sensors, electrode materials for secondary batteries, solar energy devices, photocatalysts, and field-emission devices.[4−11] Many studies have been reported[4,12−16] on the fabrication of WO_3 sensors for detecting many gases, including NO_x, H_2S, H_2, CH_3COCH_3, and so forth. However, most of the studies focused on WO_3 solid polycrystalline films which were made from large particles.[13−16] Although there were a few reports on gas-sensing properties of tungsten oxide nanorods,[17−19] these gas sensors were almost based on tungsten oxide nanorod film. For example, Kim reported the dependence of their materials (WO_3 nanorods) and gas-sensing properties on thermal treatment conditions. Liu and his co-workers reported facile synthesis and NO_2 gas sensing of tungsten oxide nanorod assembled microspheres.

Many attempts have been made to enhance the gas sensitivity of semiconductor gas sensors, one of which involved the doping of dopants in the films.[15,16,20] Penza et al. achieved a high sensitivity when noble metals such as Pt, Au, and Pd were deposited as activator layers on WO_3 films.[15,16] Kolmakov and his co-workers reported the successful and controllable sensitization of the surface of individual quasi-1-D SnO_2 nanostructures with Pd nanoparticles.[21] In practice, the photocatalytic properties are usually improved by functionalizing the material with catalytical active metals.[22−26] For example, gold-modified titania (Au/TiO_2) photocatalysts exhibited activity under visible-light (>420 nm) irradiation as reported in several papers.[24−27] Because the morphology of noble metal nanoparticles and their distribution on the surfaces of nanorods are critical to the catalytic properties,[28−31] it is highly desired to uniformly modify the surfaces of nanorods with monodispersed nanoparticles. The SnO_2 nanowires functionalized with Pd particles were produced with gas-phase approaches.[32] Inconveniently, these protocols often require high temperature and induce impurities in the final products when catalysts and templates are introduced into the reaction system, further limiting their application field. Therefore, a simple and effective solution-based synthetic strategy should be adopted.

In the present study, much research in this area has focused on the design and fabrication of functional materials with controlled structures.[33−37] In this paper, we reported a self-assembly approach for building nanoarchitectures with WO_3 nanorods (WO_3 NRs) and Au nanoparticles (Au NPs) as building blocks and further fabricating chemical sensors with highly enhanced performances. In addition, Au NP@WO_3 NRs were used as a sensing material and photocatalyst for the first time. The gas sensing properties and the photocatalytic activity of pure and Au NP@WO_3 NRs were investigated in detail, respectively. Compared with pure WO_3 NRs, Au NP@WO_3 NRs exhibit not only highly improved response and selectivity for H_2 gas detection but also high photocatalytic activity for the degradation of RhB under irradiation of simulated sunlight.

2. Experimental Section

All of the reagents were of analytical purity, purchased from Shanghai Chemical Industrial Co. Ltd. (Shanghai, China), and used as received.

2.1. Preparation of WO_3 Nanorods. The synthesis details of WO_3 NRs can be known in the literature[38] and summarized as follows: A solution containing 3.5 g of $Na_2WO_4 \cdot 2H_2O$ and 20 mL of deionized water (DI water) was loaded in a buret column, which filled with strongly acidic ion-exchange resin (Lukang Pharmaceuticals) in its proton form. A yellow tungstic acid sol was produced and dipped dropwise into a 100 mL beaker under magnetic stirring. After 1 h of the ion-exchanging process, the column was flushed with 30 mL of distilled water

* Corresponding author. Phone: +86 21 66132406. Fax: +86 21 66134594. E-mail: xujiaqiang@shu.edu.cn.
† Shanghai University.
‡ Chinese Academy of Sciences.

10.1021/jp909742d
Published on Web 01/15/2010

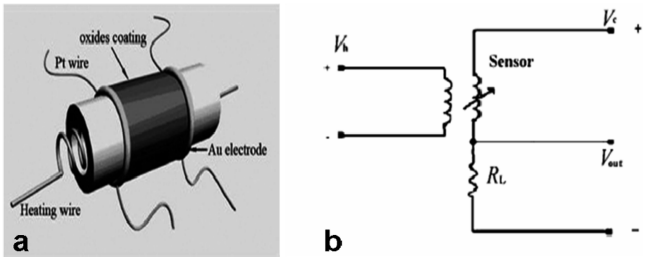

Figure 1. Sketch of the gas-sensor structure (a) and measuring electric circuit of the gas sensor (b).

and the effluent was also collected in the above 100 mL beaker. The collected opaque solution was transferred into a Teflon-lined stainless-steel autoclave of 50 mL capacity, sealed, and maintained at 180 °C for 24 h. After the hydrothermal process, the autoclave was cooled naturally to room temperature. The resulting mixture was centrifuged and washed thoroughly with ethanol and distilled water in sequence. The white precipitate can be obtained and dried at 60 °C for 12 h to form the pale yellow powders for further characterizations.

2.2. Synthesis of Au Nanoparticles. PVP-stabilized Au NPs were synthesized with a modified technique according to the literature.[39,40] An aqueous solution of $HAuCl_4$ was prepared by dissolving 0.0100 g of $HAuCl_4 \cdot 4H_2O$ into 100 mL of DI water. The solution was heated to its boiling point and kept refluxing for several hours. $HAuCl_4$ was reduced by an aqueous solution of sodium citrate (1%) in the presence of poly(vinyl pyrrolidone) (PVP) (K-30, 0.0800 g). It was observed that the solution color changed from yellow to pale yellow and finally showed purple-red. Then, the above solution was diluted to the original volume after cooling to room temperature. Au sol stabilized with PVP was obtained. For comparison, Au NPs without PVP as the protector were synthesized with the same procedure.

2.3. Preparation of Au NP@WO_3 NRs. Several milliliters of the prepared Au NP sol were mixed with WO_3 NRs (20.0 mg). The mixtures were grounded in an agate mortar for 1 h, and then dried at 100 °C for 2 h. The Au NP@WO_3 NR composites were obtained by calcinating different proportions of purple-red solids of WO_3 NRs and Au NPs (0.5, 1, and 1.5 wt %) at 500 °C for 2 h for removing PVP.

2.4. Characterization. The crystal structure of as-prepared samples was characterized by powder X-ray diffraction (XRD) on a D/max 2550 V X-ray diffractometer (Rigaku, Tokyo, Japan) with monochromatized Cu Kα ($\lambda = 1.5418$ Å) incident radiation. XRD patterns were recorded from 20 to 80° (2θ) with a scanning step of 0.02°/s. The morphologies and sizes of the samples were observed by transmission electron microscopy (TEM, JEM-200CX operated at 160 kV, JEOL JEM 2010F operated at 200 kV).

2.5. Gas-Sensing Properties Research. The structure of the gas sensor belongs to the side-heated type. The basic fabrication process is as follows: The final products were mixed and grounded with terpineol in an agate mortar to form a paste, then the paste was coated on an alumina tube-like substrate on which a pair of Au electrodes had been previously printed, followed by drying at 100 °C for 2 h and subsequent calcinating at 500 °C for 2 h. Finally, a small Ni−Cr alloy coil was placed through the tube as a heater, which provided the working temperature of the gas sensor. In order to improve the long-term stability, the sensors were kept at their working temperature for aging for several days. The gas response was measured in the static state. The gas to be tested was injected into a test bottle and mixed with air. Figure 1 shows a schematic drawing of the gas sensor and the measuring electric circuit for the gas sensor.

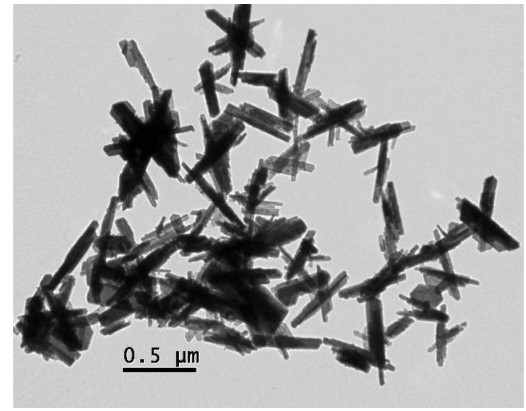

Figure 2. The TEM image of WO_3 NRs.

The working temperature of the sensors was adjusted by varying the heating voltage (V_h). By monitoring output voltage (V_{out}), the resistance of the sensor in air or test gas can be measured. Output voltage (V_{out}) is the terminal voltage of the load resistor. The gas sensitivity of the sensor in this paper was defined as $S = R_a/R_g$, where R_a and R_g were the resistance in air and test gases, respectively. The response time is defined as the time required for the sample variation conductance to reach 90% of the equilibrium value following an injection of the test gas, and the recovery time is the time necessary for the sample to return to 10% above the original conductance in air after releasing the test gas.

2.6. Photocatalytic Measurement. RhB solutions (5 mg·L^{-1}) with the appropriate amount of catalyst were magnetically stirred before and during the illumination. The suspension was agitated for 30 min in the absence of light, prior to the illumination, in order to achieve the maximum adsorption of the RhB dye onto the semiconductor surface. Then, this suspension was radiated with simulated sunlight (Xenic lamp as light source, 350 W, wavelength from 200 to 800 nm). After each given irradiation time, 5 mL of the mixture was withdrawn and separated by centrifuging to remove any suspended solids. The degradation process was monitored by a UV−vis/NIR spectrophotometer (UV-3600, Shimadzu, measuring the maximum absorption of RhB at 554 nm).

The photodegradation efficiency η was calculated by the following formula.

$$\eta = \frac{A_0 - A_i}{A_0} \times 100\%$$

Here, A_0 was the initial absorbance of RhB before reaction and A_i was the absorbance of the undegraded RhB solution after irradiation time "t_i".

3. Results and Discussion

3.1. Crystal Structure and Morphology. Tungsten trioxide nanorods were prepared by an ion-exchange method combined with hydrothermal treatment. From the TEM images of WO_3 NRs (Figure 2), it is found that the product mainly consists of nanorods with a diameter of 50−80 nm and length of 500 nm. Figure 3 is a representative XRD pattern of the synthesized WO_3 NRs. The WO_3 NRs are of typical wurtzite (hexagonal) structure with lattice constants of $a = b = 0.7298$ nm and $c = 0.3899$ nm. All of the WO_3 NR diffraction peaks in Figure 3 can be well indexed to the standard pattern of WO_3 (JCPDS No. 33-1387).

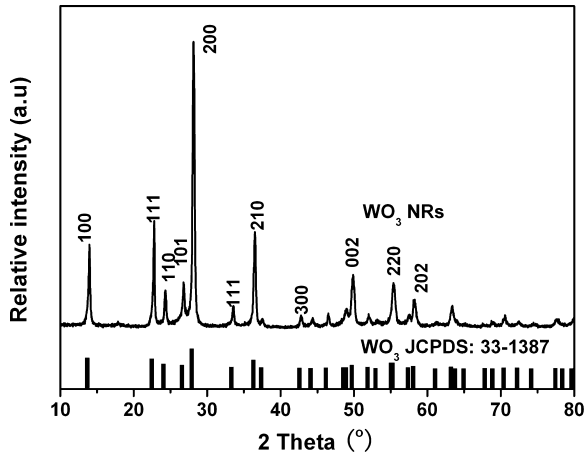

Figure 3. XRD pattern of WO_3 NRs.

Au NPs were prepared by a chemical reductive process with sodium citrate as a reductive agent. From the TEM image of the Au NPs (Figure 4a), it was found that monodispersed Au NPs with a diameter of about 10 nm were synthesized successfully.

WO_3 NRs with different Au loadings (0.5, 1, 1.5, 3, and 5 wt %) were prepared by mixing Au sol with WO_3 NRs and annealed at 500 °C. This procedure resulted in a highly uniform dispersion of Au particles (average size, 10 nm) on the WO_3 surface.

Figure 4b,c shows a low magnification TEM image of WO_3 NRs modified with 0.5 wt % Au NPs. Compared with the pure Au NPs (Figure 4a), a number of Au NPs with an average diameter of about 10 nm decorated the WO_3 NR surface. Comparing the effect of PVP on Au particle size, it is obvious that more Au NPs homogeneously deposited on the surfaces of WO_3 NRs when PVP was employed in the synthesis system (Figure 4b) than that without PVP (Figure 4c). PVP played an important role not only in stabilizing Au NPs but also in anchoring Au NPs onto the surfaces of the WO_3 NRs through coordinative bonding, thus the composite with uniform and well dispersion of Au NPs on WO_3 NRs obtained.[39]

Figure 5 shows the XRD patterns of pure WO_3 and WO_3 NRs with different Au loadings after annealing, confirming decoration of Au NPs onto WO_3 NRs. The XRD pattern of the sample being annealed for 2 h at 500 °C is a typical monoclinic WO_3 phase, which is indexed well with the XRD pattern of monoclinic WO_3 (JCPDS file No. 43-1035). No apparent peaks of gold can be observed at a low concentration of gold loading (0.5 wt %) because low gold diffraction intensity was hidden by WO_3. When the amount of gold nanoparticles is increased to 3 wt %, the diffraction peaks of gold become obvious and sharper. The intensity is further increased when the amount of gold loading reaches 5 wt %. Moreover, the XRD patterns confirmed that the WO_3 phase and Au phase exist in the 5 wt % Au NP@WO_3 NR composite.

3.2. Gas-Sensing Properties of the Sensor. Several kinds of reducing gases, including H_2, CO, C_2H_5OH, CH_3OH, HCHO, and NH_3 with a gas concentration of 50 ppm were used as detecting gases to characterize the gas sensing properties of the NP@WO_3 NR composite. The test was operated in a measuring system of HW-30A (Hanwei Electronics Co. Ltd., Henan, China). The gas sensitivity was measured in the static state.

The sensing characteristic of WO_3 for a special gas is usually dependent on the temperature, so in this paper, parallel experiments were carried out in the range 200−400 °C to optimize the working temperature of the sensors fabricated. The results indicate that the Au NP@WO_3 NR composite shows the highest response (Figure 6) to hydrogen at 290 °C. Then, 290 °C was fixed to be the working temperature to proceed with the subsequent detections.

We further investigated the density effect of Au NPs on the surfaces of WO_3 NRs to the functionalities of chemical sensors (Figure 7). The chemical sensors constructed with Au NP@WO_3 NRs exhibited improved performances when compared with that made with pure WO_3 NRs (Figure 7). The response sensitivity (Ra/Rg) of Au NP@WO_3 NRs is up to 6.6, after increasing Au NP loadings on the surfaces of WO_3 NRs to 0.5 wt % and exposed to H_2 gas of 50 ppm. However, further loading more Au NPs onto the surfaces of WO_3 NRs leads to lowering of the responses of chemical sensors. Monodispersed Au NPs have remarkable influences on the performances of sensors after uniformly attaching onto the surfaces of WO_3 NRs. The active surfaces of WO_3 NRs could also affect the functionalities of chemical sensors. Too much Au NPs blotting out the active sites of WO_3 NRs caused a decrease of the responses of H_2 sensors, and the cost of the sensor is also a problem that we should consider. Thus, the optimized amount of Au NPs on the surfaces of WO_3 NRs is 0.5 wt % for its high sensitivity to the test 50 ppm H_2 gas.

Figure 8 shows the gas sensing performance of Au NP@WO_3 NRs and pure WO_3 NRs at an optimal operating temperature of 290 °C. The sensitivity of Au NP@WO_3 NR sensors (Figure 8) to all of the measured gases is higher than that of sensors from pure WO_3 NRs.

The sensitivity of the Au NP@WO_3 NR sensor (Figure 8) is 6.6 to H_2 of 50 ppm, much higher than that of other gases and nearly 4 times as high as that of the pure WO_3 NR sensor. The H_2 concentration (50 ppm) is much lower than the explosive limit value of hydrogen in our living environment (4000 ppm), which indicates a potential application of H_2 sensor with high sensitivity.

In addition, stability is a property that must be considered and verified as being acceptable if a gas sensor is to be used for practical applications.[41] The stability of Au NP@WO_3 NR sensors illustrated in Figure 9a indicates that the responses of sensors have not obviously descended after being exposed in 50 ppm H_2 for 56 days and the sensitivity slowly descends from 6.5 to 5.9 and maintains a stable value, indicating that the prepared Au NP@WO_3 NR sensors exhibit high long-term stability in their response and selectivity for detecting H_2 gas.

The variations of the response voltage of Au NP@WO_3 NR sensors with hydrogen concentration ranging from 50 to 1000 ppm are shown in Figure 9b. The response voltage of sensors increases with the increase of H_2 concentration and the response/recovery time is very short, which means that the reversibility and repeatability for the gas sensors are very perfect.

Impregnation is a conventional method for adding noble metals onto the surfaces of WO_3 NRs and improving the performances of chemical sensors. In order to better understand the reasons of highly improved performances of H_2 sensors that are produced by Au NPs decorating on WO_3 NRs, we processed the surface modification of WO_3 NRs with impregnation by adding $HAuCl_4$ solution (0.5 wt %) onto WO_3 NRs (named Au-WO_3 NRs) and annealing at 500 °C.

Figure 10 shows the dynamic responses of three sensors constructed with pure WO_3 NRs, Au-WO_3 NRs, and Au NP@WO_3 NRs, respectively. It was obvious that the performances of the sensors can all be enhanced by loading Au onto the surfaces of WO_3 NRs; the response of Au NP@WO_3 NR sensors is the highest and almost twice higher than that of those

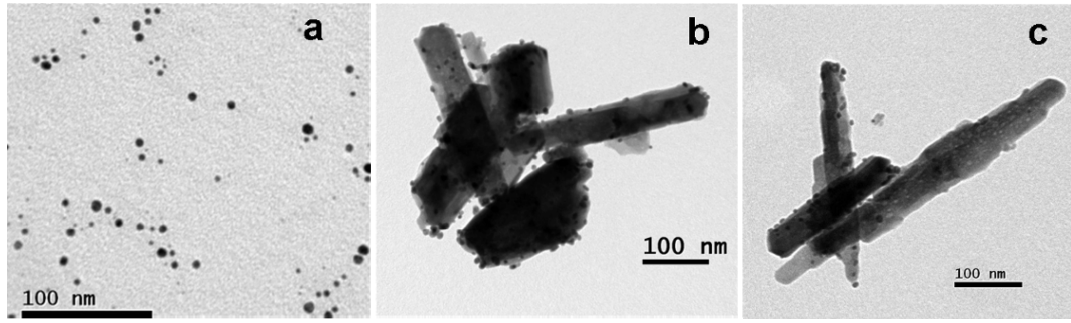

Figure 4. TEM images of Au NPs (a) and 0.5 wt % Au NP @WO_3 NRs (b) with and (c) without PVP as a protecting agent.

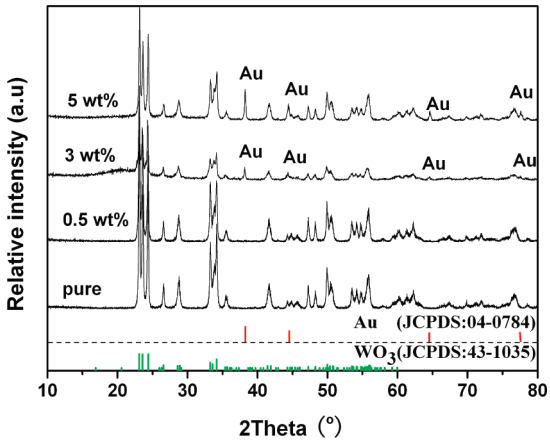

Figure 5. XRD patterns of pure WO_3 and Au NP@WO_3 NRs with different Au loadings, with annealing at 500 °C for 2 h.

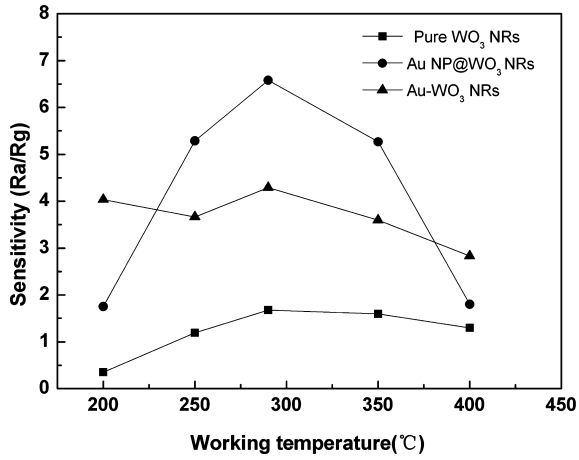

Figure 6. Temperature dependence of sensor sensitivity to hydrogen at 50 ppm.

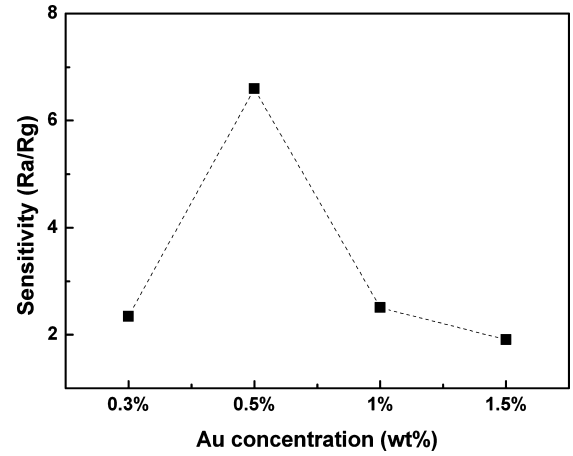

Figure 7. Au concentration as a function of the 50 ppm H_2 on WO_3 NRs under 4.5 V.

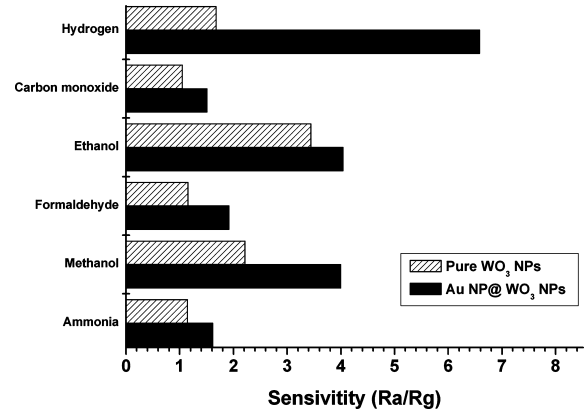

Figure 8. Gas sensing performance of Au NP@WO_3 NRs to different gases of 50 ppm.

made from Au-WO_3 NRs. The response and recovery time of Au NP@WO_3 NRs to H_2 of 50 ppm were only 8 and 10 s, respectively. The response time is the time needed for the conductance of the gas sensor to obtain 90% of the maximum conductance when H_2 gas is introduced into the environment of air.

In a recent report, Joshi et al. have suggested a mechanism to understand the change in resistance by using CO adsorption/disorption on the surface of Au nanocrystals@ZnO nanowires.[42] They suggested that oxygen absorption/desorption and electron transfer affect the conductance of ZnO nanowires. The conductive Au nanocrystals spill the gas over the semiconductor surface via the spillover effect, and the catalytic activation and chemical sensitization were observed to be responsible for CO sensing by Au NP modified ZnO nanowires. It is well-known[18,19,43] that oxygen absorption has an important effect on electrical transport properties of WO_3 nanorods. It is also known[17,44] that oxygen ionsorption removes conduction electrons and thus lowers the conductance of WO_3. The conductive nanocrystals spill the gas over the semiconductor surface via the spillover effect.[42] In the case of the synthesized Au NP@WO_3 NR composite, a similar spillover effect[45,46] also can be employed to illustrate the H_2 sensing properties on the Au NP@WO_3 NR composite. It was worth noting that Au particles not only catalyze O_2 dissociation but also catalyze H_2 dissociation on its surface,[47] which may cause a high sensitivity of H_2.

Thus, we suggested the H_2 reaction kinematics in Figure 11. As shown in step 1, when WO_3 nanorods are exposed to air, oxygen molecules can adsorb on the surface of the nanorod and form O_2^- ions by capturing electrons from the conductance band. In step 2, when the sensor is exposed to H_2, the H_2

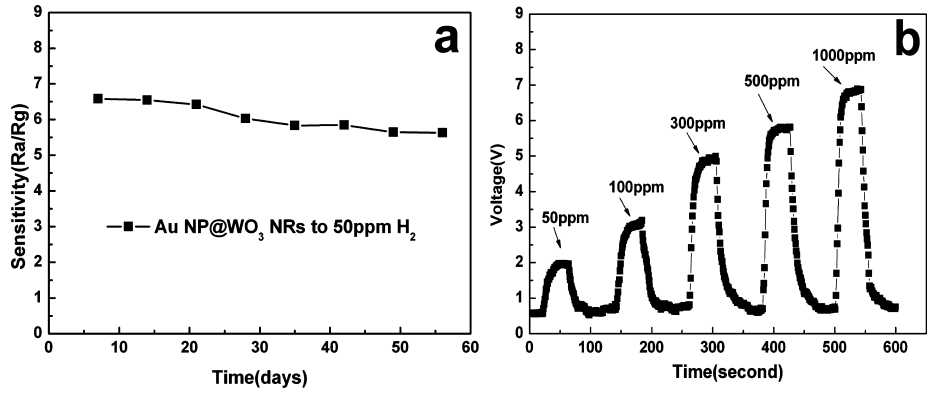

Figure 9. Stability (a) and typical voltage response variations (b) of Au NP@WO_3 NR (Au loading 0.5 wt %) sensors exposed to H_2 at concentrations ranging from 50 to 1000 ppm and measured at 290 °C.

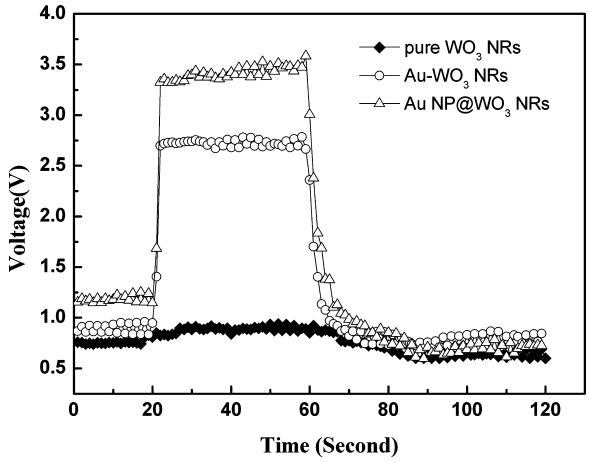

Figure 10. Dynamic response of different samples to 50 ppm H_2.

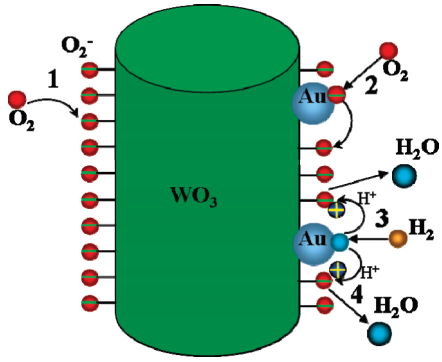

Figure 11. Mechamism of H_2 reaction on the Au NP@WO_3 NR sensor.

molecules on the Au surface were dissociated to be H atom, which corresponding to the step 3. At step 4, H atoms dissociated by Au particles transfer to the surface of WO_3 and interact with the preadsorbed oxygen ions. Hence, the H_2 oxidation by gold nanocrystals leads to the transfer of electrons in semiconductive WO_3 NRs in terms of a change in resistance of the sensing material. The grain interface resistance descends, which confirms that the sensitivity of H_2 sensors made from Au NP@WO_3 NRs is much better than pure WO_3 NPs.

3.3. Photocatalytic Activity. The photocatalytic activity of Au NP@WO_3 NRs was also rated with the photocatalytic degradation of RhB under irradiation of simulated sunlight.

UV−vis absorbance spectra for pure WO_3, Au NPs, and Au NP@WO_3 NRs are shown in Figure 12. Both WO_3 and Au NP@WO_3 NRs have intense absorption in the near-ultraviolet

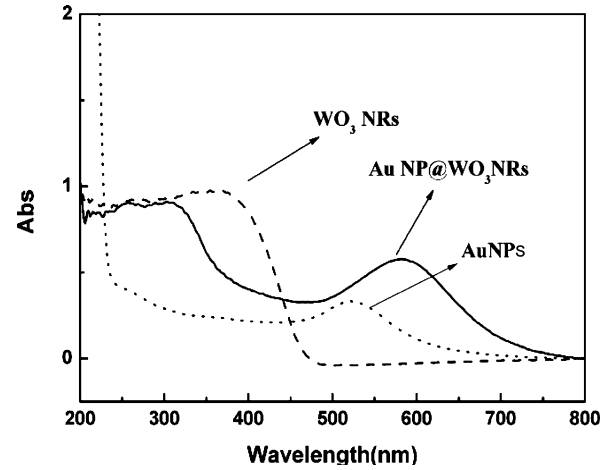

Figure 12. UV−vis absorbance spectra of pure WO_3 and Au NP@WO_3 NRs.

region (from 270 to 450 nm), which should be attributed to high UV absorbance of WO_3. Differently, in the visible light region (450−800 nm), the Au NP@ WO_3 NR composite shows strong vis absorbance with a strong absorbance peak at 582 nm; pure Au NPs also have strong vis absorbance at 525 nm. However, no obvious vis absorbance was shown for pure WO_3. The absorption wavelengths of UV−vis spectra for Au NP@WO_3 NR samples at 305 and 582 nm exhibited an obvious red shift in contrast to that of Au nanoparticles and a blue shift in contrast to that of pure WO_3 NRs, respectively. This result confirmed that Au NP@ WO_3 NRs can strongly absorb visible light and ultraviolet light simultaneously and indicated that the Au NP@ WO_3 NR composite has a potential application of RhB photodegradation in sunlight.

The photodegradation efficiency (η) of RhB for Au NP@WO_3 NR catalysts was monitored to measure the photocatalytic activity (Figure 13). The η value of Au NP@WO_3 NRs is higher than that of pure WO_3 NRs under the same conditions. Photodegradation of RhB solution under simulated sunlight with Au NP@WO_3 NRs as the catalyst is almost complete in 120 min. The high photodegradation ability of RhB would be attributed to high monodispersed Au NPs, which could effectively separate the photogenerated electron−hole pairs by trapping the charge carrier, as well as band gap excitation of tungsten trioxide and the activity−structure correlation. Such a result corresponds to the literature,[48−55] in which noble metals loading on the surface of semiconductor could trap the charge carriers.

The following photocatalysis mechanism of Au NP@WO_3 NRs is proposed (Figure 14). First, incident photons are absorbed

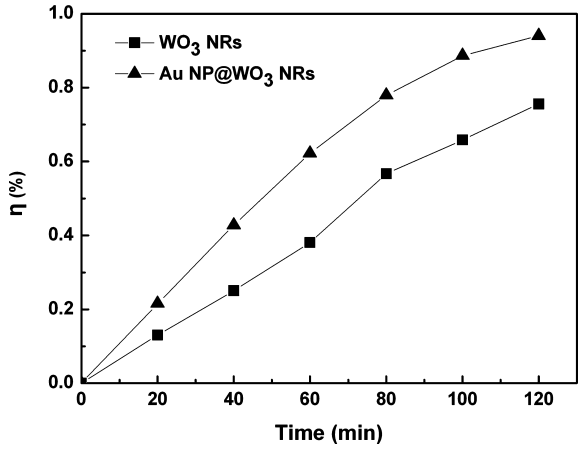

Figure 13. Photodegradation of RhB solution using pure WO_3 NRs and 0.5 wt % Au NP@WO_3 NRs under simulated sunlight.

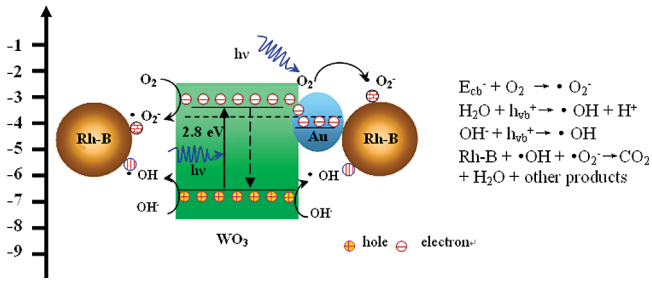

Figure 14. Mechamism of RhB photodegradation on Au NP@WO_3 NRs composite.

TABLE 1: Variation of Response/Recovery Time and Sensitivity of H_2 with Au Concentration, Operating Temperature (290 °C), and H_2 Concentration (50 ppm)

Au concentration (wt %)	response time (s)	recovery time (s)	sensitivity (Ra/Rg)
0.3	16	18	2.346
0.5	8	10	6.60
1.0	8	14	2.511
1.5	33	32	1.908

by Au NPs. Band gap excitation occurred in WO_3 after photon excitation and photoelectrons in the valence band were excited to the conductive band with simultaneous generation of the same amount of holes (h_{vb}^+) in the valence band. Partial photoexcited electrons would transfer from WO_3 to Au because of the lower Fermi energy of Au metal; thus the coupling between electrons and holes was restrained. Because the Au NP@WO_3 NR composite can absorb light in a wider wavelength range from the near-ultraviolet region to visible light, leading to a larger number of absorption photons and more electrons would be excited from WO_3, in further, more amount of holes obtained. The oxygen molecule received electrons and formed superoxide anions ($\bullet O_2^-$); simultaneously, the photoinduced holes were trapped by OH^- to form hydroxyl radicals. More superoxide anions and hydroxyl radicals formed on the surface of Au NP@WO_3 NR composites would oxidize RhB with a high photodegradation rate.

4. Conclusion

In summary, we have presented a special method for uniformly attaching monodispersed Au NPs onto the surfaces of WO_3 NRs used as H_2 sensors with highly enhanced response and selectivity for the first time and high photocatalytic activity composite for the degradation of organic dye RhB. The response and recovery time of the sensor to H_2 of 50 ppm were only 8 and 10 s, respectively, which means a high selectivity and response sensitivity of H_2 on the Au NP@WO_3 NR composite. Also, the synthesized Au NP@WO_3 NR composite exhibits high photocatalytic activity for the decomposition of RhB solution under irradiation of simulated sunlight. It is generally considered that monodispersed Au NPs act as a catalyst not only in the gas response but also in the photocatalytic activity. In addition, the UV−vis spectroscopy of all the samples confirmed that Au NP@WO_3 NRs can absorb more UV−visible light than pure WO_3 NRs. Therefore, Au NP@WO_3 NRs would have a widely applied prospect in the UV−visible light driven photocatalyst field. The availability of nanosized building blocks with highly controlled nanostructures, such as nanorods and nanoparticles of noble metals and semiconductors, enables us to construct diverse functional nanoarchitectures for fabricating gas sensors with tunable performances. Further study about this work is in progress in our lab.

Acknowledgment. We appreciate the sponsorship by Shanghai NSF (No. 07ER14039) and Leading Academic Discipline Project of Shanghai Municipal Education Commission (No. J50102). We also thank the Analysis and Research Center at Shanghai University for sample characterization.

References and Notes

(1) Yoo, S. J.; Lim, J. W.; Sung, Y. E.; Jung, Y. H.; Choi, H. G.; Kim, D. K. *Appl. Phys. Lett.* **2007**, 173126.
(2) He, T.; Ma, Y.; Cao, Y. A.; Yang, W. S.; Yao, J. N. *Phys. Chem. Chem. Phys.* **2002**, *4*, 1637.
(3) Lu, Y. M.; Hu, C. P. *J. Alloys Compd.* **2008**, *449*, 389.
(4) Nagata, S.; Inouye, A.; Yamamoto, S.; Tsuchiya, B.; Takano, K.; Toh, K.; Shikama, T. *J. Alloys Compd.* **2007**, *446*, 558.
(5) Jing, L. Q.; Wang, D. J.; Wang, B. Q.; Li, S. D.; Xin, B. F.; Fu, H. G.; Sun, J. Z. *J. Mol. Catal. A: Chem.* **2006**, *244*, 193.
(6) Lou, X. W.; Zeng, H. C. *Inorg. Chem.* **2003**, *42*, 6169.
(7) Teoh, L. G.; Shieh, J.; Lai, W. H.; Hung, I. M.; Hon, M. H. *J. Alloys Compd.* **2005**, *396*, 251.
(8) He, T.; Ma, Y.; Cao, Y.; Hu, X. L.; Liu, H. M.; Zhang, G. J.; Yang, W. S.; Yao, J. N. *J. Phys. Chem. B* **2002**, *106*, 12670.
(9) Hibino, M.; Han, W. C.; Kudo, T. *Solid State Ionics* **2000**, *135*, 61.
(10) Zhang, B.; Liu, J. D.; Guan, S. K.; Wan, Y. Z.; Zhang, Y. Z.; Chen, R. F. *J. Alloys Compd.* **2007**, *439*, 55.
(11) Ha, J. H.; Muralidharan, P.; Kim, D. K. *J. Alloys Compd.* **2009**, *475*, 446.
(12) Shimizu, Y.; Matsunaga, N.; Hyodo, T.; Egashira, M. *Sens. Actuators, B* **2001**, *77*, 35.
(13) Boulova, M.; Gaskov, A.; Lucazeau, G. *Sens. Actuators, B* **2001**, *81*, 99.
(14) Wang, L.; Teleki, A.; Pratsinis, S. E.; Gouma, P. I. *Chem. Mater.* **2008**, *20*, 4794.
(15) Penza, M.; Martucci, C.; Cassano, G. *Sens. Actuators, B* **1998**, *50*, 52.
(16) Penza, M.; Cassano, G.; Tortorella, F. *Sens. Actuators, B* **2001**, *81*, 115.
(17) Kim, Y. S.; Lee, K. *J. Nanosci. Nanotechnol.* **2009**, *9*, 2463.
(18) Liu, Z. F.; Miyauchi, M.; Yamazaki, T.; Shen, Y. B. *Sens. Actuators, B* **2009**, *140*, 514.
(19) Kim, Y. S. *Sens. Actuators, B* **2009**, *137*, 297.
(20) Xia, H. J.; Wang, Y.; Kong, F. H.; Wang, S. R.; Zhu, B. L.; Guo, X. Z.; Zhang, J.; Wang, Y. M.; Wu, S. H. *Sens. Actuators, B* **2008**, *134*, 133.
(21) Kolmakov, A.; Klenov, D. O.; Lilach, Y.; Stemmer, S.; Moskovits, M. *Nano Lett.* **2005**, *5*, 667.
(22) Abe, R.; Takami, H.; Murakami, N.; Ohtani, B. *J. Am. Chem. Soc.* **2008**, *130*, 7780.
(23) Kowalska, E.; Abe, R.; Ohtani, B. *Chem. Commun.* **2009**, 241.
(24) Tian, Y.; Tatsuma, T. *J. Am. Chem. Soc.* **2005**, *127*, 7632.
(25) Rodriguez-Gonzalez, V.; Zanellac, R.; del Angela, G.; Gomeza, R. *J. Mol. Catal. A: Chem.* **2008**, *281*, 93.
(26) Sonawane, R. S.; Dongare, M. K. *J. Mol. Catal. A: Chem.* **2006**, *243*, 68.
(27) Ohtani, B. *Chem. Lett.* **2008**, *37*, 216.

(28) Li, L. M.; Li, C. C.; Zhang, J.; Du, Z. F.; Zou, B. S.; Yu, H. C.; Wang, Y. G.; Wang, T. H. *Nanotechnology* **2007**, *18*, 225504.
(29) Potje-Kamloth, K. *Chem. Rev.* **2008**, *108*, 367.
(30) Kang, W. P.; Kim, C. K. *Sens. Actuators, B* **1994**, *22*, 47.
(31) Morrison, S. R. *Sens. Actuators, B* **1987**, *12*, 425.
(32) Sze, S. M. *Semiconductor Sensors*; Wiley: New York, 1994; p 384.
(33) Li, F.; Badel, X.; Linnros, J.; Wasserman, G.; Whittenburg, S. L.; Spinu, L.; Wiley, J. B. *Adv. Mater.* **2006**, *18*, 270.
(34) Li, F.; Badel, X.; Linnros, J.; Wiley, J. B. *J. Am. Chem. Soc.* **2005**, *127*, 3268.
(35) Li, F.; He, J. B.; Zhou, W. L. L.; Wiley, J. B. *J. Am. Chem. Soc.* **2003**, *125*, 16166.
(36) Li, F.; Wiley, J. B. *J. Mater. Chem.* **2008**, *18*, 3977.
(37) Li, F.; Xu, L. B.; Zhou, W. L. L.; He, J. B.; Baughman, R. H.; Zakhidov, A. A.; Wiley, J. B. *Adv. Mater.* **2002**, *14*, 1528.
(38) Mo, R. F.; Jin, G. Q.; Guo, X. Y. *Mater. Lett.* **2007**, *61*, 3787.
(39) Zhang, J. H.; Liu, H. Y.; Zhan, P.; Wang, Z. L.; Ming, N. B. *Adv. Funct. Mater.* **2007**, *17*, 1558.
(40) Wu, H. Y.; Huang, W. L.; Huang, M. H. *Cryst. Growth Des.* **2007**, *7*, 831.
(41) Qin, L. P.; Xu, J. Q.; Dong, X. W.; Pan, Q. Y.; Cheng, Z. X.; Xiang, Q.; Li, F. *Nanotechnology* **2008**, *19*, 185705.
(42) Joshi, R. K.; Hu, Q.; Am, F.; Joshi, N.; Kumar, A. *J. Phys. Chem. C* **2009**, *113*, 16199.
(43) Kim, Y. S.; Ha, S. C.; Kim, K.; Yang, H.; Choi, S. Y.; Kim, Y. T. *Appl. Phys. Lett.* **2005**, *86*, 213105.
(44) Tamaki, T.; Zhang, Z.; Fujimori, K.; Akiyama, M.; Harada, T.; Miura, N.; Yamanoe, N. *J. Electrochem. Soc.* **1994**, *141*, 2207.
(45) Joshi, R. K.; Einar Kruis, F.; Dmitrieva, O. *J. Nanopart. Res.* **2006**, *8*, 797.
(46) Yamazoe, N. *Sens. Actuators, B* **1991**, *5*, 7.
(47) Gossner, K.; Mansfeld, F. *Z. Phys. Chem.* **1968**, *58*, 19.
(48) Gouvea, C. A. K.; Wypych, F.; Moraes, S. G.; Duran, N.; Peralta-Zamora, P. *Chemosphere* **2000**, *40*, 427.
(49) Height, M. J.; Pratsinis, S. E.; Mekasuwandumrong, O.; Praserthdam, P. *Appl. Catal., B* **2006**, *63*, 305.
(50) Zhou, G.; Deng, H. C. *Mater. Sci. Semicond. Process.* **2007**, *10*, 90.
(51) Chen, T. W.; Zheng, Y. H.; Lin, J. M.; Chen, G. N. *J. Am. Soc. Mass Spectrom.* **2008**, *19*, 997.
(52) Subramanian, V.; Wolf, E. E.; Kamat, P. V. *J. Phys. Chem. B* **2003**, *107*, 7479.
(53) Abe, T.; Suzuki, E.; Nagoshi, K.; Miyashita, K.; Kaneko, M. *J. Phys. Chem. B* **1999**, *103*, 1119.
(54) Subramanian, V.; Wolf, E.; Kamat, P. V. *J. Phys. Chem. B* **2001**, *105*, 11439.
(55) Teoh, W. Y.; Madler, L.; Beydoun, D.; Pratsinis, S. E.; Amal, R. *Chem. Eng. Sci.* **2005**, *60*, 5852.

JP909742D